Applied Physics Letters ARTICLE scitation.org/journal/apl

Observation of multilayer-structured discharge in plasma ionization breakdown

Cite as: Appl. Phys. Lett. **119**, 264102 (2021); doi: 10.1063/5.0076519
Submitted: 25 October 2021 · Accepted: 8 December 2021 ·
Published Online: 28 December 2021

De-Qi Wen,[1,2,a)] Peng Zhang,[1] Janez Krek,[2] Yangyang Fu,[3] and John P. Verboncoeur[1,2]

AFFILIATIONS

[1]Department of Electrical and Computer Engineering, Science and Engineering, Michigan State University, East Lansing, Michigan 48824, USA
[2]Department of Computational Mathematics, Science and Engineering, Michigan State University, East Lansing, Michigan 48824, USA
[3]Department of Electrical Engineering, Tsinghua University, Beijing 100084, China

[a)]Author to whom correspondence should be addressed: wendeqi@msu.edu

ABSTRACT

In this Letter, a multilayer-structured discharge (MSD) is reported in multipactor-coexisting plasma ionization breakdown by fully kinetic particle-in-cell simulations. The observed multilayer structure is originated by the response of ions to an electric field. It is found that the electron diffusion and multipactor discharge near the surface produce two opposite electric fields toward and away from the dielectric surface, respectively. Thus, the ions form a locally high density profile, which is followed by electron density. The lighter electrons diffuse away from the peak more quickly than the ions, resulting in an ambipolar field toward the bulk plasma region, which drives the ion density peak to propagate toward the bulk plasma. Such a process is periodically repeated, and, finally, a MSD is formed.

Gas ionization breakdown and multipactor discharge near a dielectric surface are of high importance in high power microwaves, which are important to many fields, including low temperature plasma processing of materials, space-based energy transmission and propulsion, cyclotron heating in fusion energy, and rf accelerators.[1–6] Especially, at higher microwave power, a plasma discharge near the microwave window can be easily triggered and negatively affects microwave transmission. Additionally, energetic electron induced multipactor, i.e., intense secondary electron emission, has been found to be important in the process of the plasma–surface interaction. Therefore, multipactor and gas ionization breakdown near a dielectric surface have attracted substantial research efforts in recent years.[7–13]

In vacuum and less collisional regimes, the discharge is dominated by the electron-surface multipacting process, during which energetic electrons repeatedly strike the dielectric surface to yield an electron avalanche.[7–9,14,15] Meanwhile, the positive charge is left on the surface and induces a normal restoring electric field, which forces the electrons to return to the dielectric surface. In recent years, multipactor susceptibility,[13,16,17] its temporal physical dynamics,[18–20] and possible mitigation to improve breakdown threshold[15,21–25] have been extensively studied. With the presence of background gas or desorbed gas from the surface due to electron bombardment, multipactor dynamics can be significantly altered by electron–neutral collisions.[26] With increasing pressure to the near-atmospheric pressure, where the electron–neutral collision frequency is much higher than the driving frequency, the emitted secondary electrons lose a significant amount of energy during flight, and the insufficient impact energy fully suppresses the surface multipacting process over time.[27] In the intermediate pressure regime (hundreds of mTorr–to a few Torr), multipactor and ionization plasma discharge can coexist.[27] Even though the scaling law of discharge formation time was studied by Neuber *et al.*[28] and Lau *et al.*,[29] the transient volume physics of the multipactor transition to ionization breakdown is barely studied in the literature and not well understood.[27] Moreover, it is of importance to understand the process of plasma breakdown when the community tries to control or avoid gas ionization breakdown near the dielectric window. Additionally, the high-power microwave system has important applications in space-based communication satellites, which usually locate in complicated space environments, such as solar wind and a proton/electron belt consisting of a vast number of electrons and helium (and protons).[30–32] These particles can be adsorbed to the microwave window surface initially and desorbed to gas around the window surface due to later surface heating.[33,34] Understanding the desorbed gas induced ionization breakdown in helium or hydrogen is important for

controlling or mitigating gas discharge near microwave windows for space-based communication satellites.

In this Letter, we report a multilayer-structured discharge (MSD) in multipactor-coexisting plasma ionization breakdown, and the regime of MSD formation is also revealed. To present the main physics, a movie showing the evolution of the spatial electron and ion density profiles in time is provided in the supplementary material. The present work is conducted by fully kinetic particle-in-cell (PIC) simulations, which are well benchmarked against other codes in the literature[35–37] and experimentally validated[38] in plasma discharge. We emphasize that the MSD is found for He in a certain range of electric field amplitudes, gas pressure, and various secondary emission properties. To reveal the most important physics, we mainly present a typical case at frequency 1 GHz, gas pressure 1.5 Torr, and rf electric field amplitude $E_0 = 3 \times 10^6$ V/m, which was commonly adapted in previous works.[18,27,29,39,40] The pressure chosen here is close to the pressure suggested by a dielectric/vacuum gas ionization breakdown experiment.[15]

The schematic of the discharge system is shown in Fig. 1, where the discharge is bounded by a dielectric surface at $x = 0$. The right boundary is semi-infinite. The rf electric field is in the y direction, tangential to the surface. The interactions between charged and neutral particles, including e-He elastic scattering, electron impact excitation and ionization, backwards and isotropic portion of He^+ and He scattering and charge exchange collisions are treated by a Monte Carlo scheme incorporating the null collision method.[41] The details about the collision threshold and corresponding cross sections can be found in Ref. 42. The charged particles flowing to the dielectric surface are also instantaneously accumulated. Primary electrons induce secondary electron emission from the surface, which is described by the well-known Vaughn's empirical formula[43] for a dull surface with smooth factor $k_s = 1$ and the maximum secondary electron yield (SEY) $\delta_{max0} = 3.0$ at the normal incidence for impact energy $E_{max0} = 400.0$ eV, similar to the treatment in previous works.[18,19,25,27] An illustration of the electron-induced secondary electron yield (SEY) in terms of the impact energy is shown in the inset of Fig. 1. Both the space charge and surface charge effects are included in our simulation.

The space-dependent transient physics is revealed by the spatiotemporal plot of normal electric field, E_x, electron density, n_e, ion density, n_i,

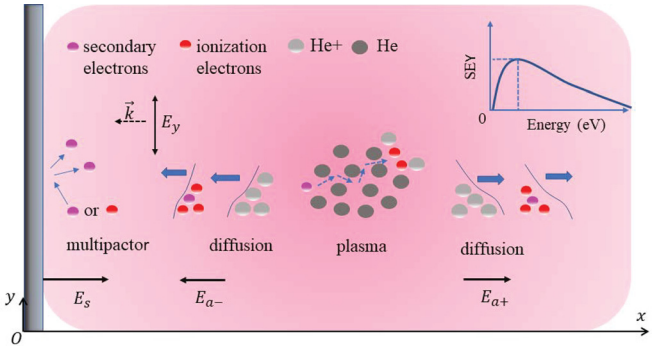

FIG. 1. Schematic diagram of the multipactor-coexisting plasma breakdown system in He with inset illustrating the secondary electron yield vs the impact energy of primary electrons at normal incidence. E_s represents the restoring field induced by the multipactor discharge and E_{a-} and E_{a+} represent the ambipolar field due to the lighter electron diffusion toward and away from the dielectric surface, respectively.

and electron–neutral ionization impact rate, R_i in Figs. 2(a)–2(d), accordingly. At the beginning of the discharge, E_x increases rapidly due to secondary electron avalanche emission from the surface and then periodically oscillates at twice the fundamental rf frequency (1 GHz) for the first three rf periods as shown in Fig. 2(a), similar to the multipactor process in vacuum.[18,20] Due to the residence of the net positive charge on the surface after electrons are ejected, the normal electric field points away from the surface everywhere and gradually decays in space under the shielding of the electron space charge effect. The electron–neutral ionization collisions result in the formation of the bulk plasma 4–60 μm in front of the dielectric as shown in Figs. 2(b) and 2(c).

Most importantly, the physics, reported here is that remarkable propagating multilayer-structured discharges are observed for the electric field, electron density, and especially ion density. This propagating behavior is clear in the movie provided in the supplementary material. The MSD expands into the bulk plasma region in time. In general, low temperature discharge characteristics are determined by electron–neutral collision dynamics, as the ion mass is too large to respond to the very high frequency oscillating electric field, i.e., $\omega_{rf} \gg \omega_{pi}$. However, for helium plasma breakdown near an emissive dielectric window, the motion of ions is found to play an important role by analyzing the electron ionization impact rate distribution, which is revealed in Fig. 2(d). As one can see, even though the ionization rate R_i shows a locally high distribution near the surface, obviously, the peak value of this locally high R_i is lower than that in the space range of 10–100 μm, implying that there would be a lower ion density near the surface in the absence of ion motion. However, the ion density in the multilayer structure near the surface (<10 μm) is much higher than that in 10–100 μm. Therefore, locally high ionization rate is not the reason for the formation of propagating MSD. Indeed, for a driving electric field at 3 MV/m, typically, the induced normal restoring field can be as high as a few MV/m as shown in Fig. 2(a). For a normal electric field of $E_x = 1$ MV/m, a static ion of helium can pass through a distance of a few μms without collisions in 1 ns due to the relatively light mass, which is non-negligible in a typical discharge size of tens of μm. Next, we will analyze the discharge dynamics, especially the regime of MSD generation in the presence of ion motion.

The analysis of the nature of the propagating MSD is based on ion mass reduction to proton mass with collision mechanics kept the same as in helium gas. The electron-relevant processes, such as electron–surface interaction (multipactor process) and electron–neutral collision and transport dynamics, are kept unchanged. In the proton system, the MSD is reproduced and more visible for analysis.

Figures 3(a)–3(i) exhibit spatiotemporal plots of the normal electric field, charged particle density, fluid velocity, and flux. The region analyzed in detail is spatially confined within 1.75–30 μm over the time duration of 4–9 rf periods, in which the MSD is typically present. The normal electric field starts showing the first propagating pattern at $t/T = 6.15$, as the red arrow shows in Fig. 3(a). The red vertical dashed line labeled by phase 1 indicates a transition at $t/T \approx 6.15$ for the three columns. Similarly, the ion density n_i, net charge density ρ, ion fluid velocity v_i, and ion flux $\Gamma_i = n_i v_i$ present the same behavior, instantaneously [see Figs. 3(b), 3(d), 3(e), and 3(h), respectively]. However, the ionization electron density n_{ie} (impact ionization produced electrons), secondary electron density n_{se} (surface emission electrons), and the corresponding ionization electron fluid velocities v_{ie}, as well as total ionization impact rate R_i have similar behavior only after

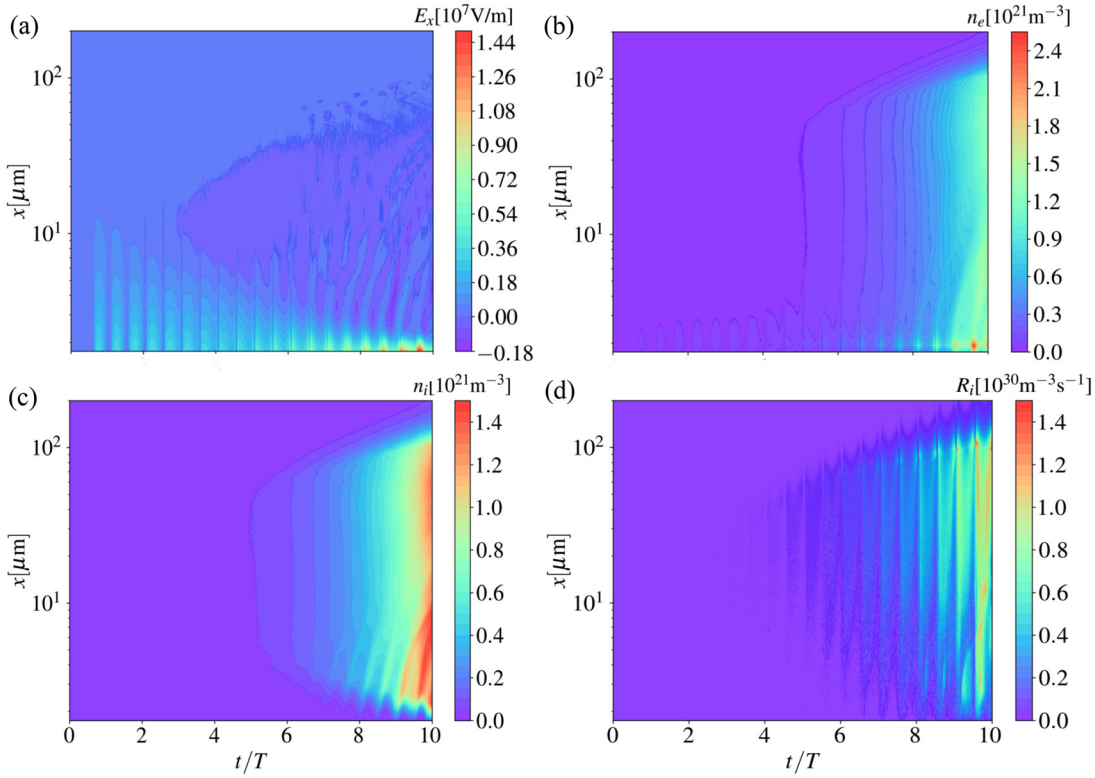

FIG. 2. Spatiotemporal plots of the multilayer structured discharge. (a) Normal electric field, (b) electron density, (c) ion density, and (d) ionization rate. T is the rf period.

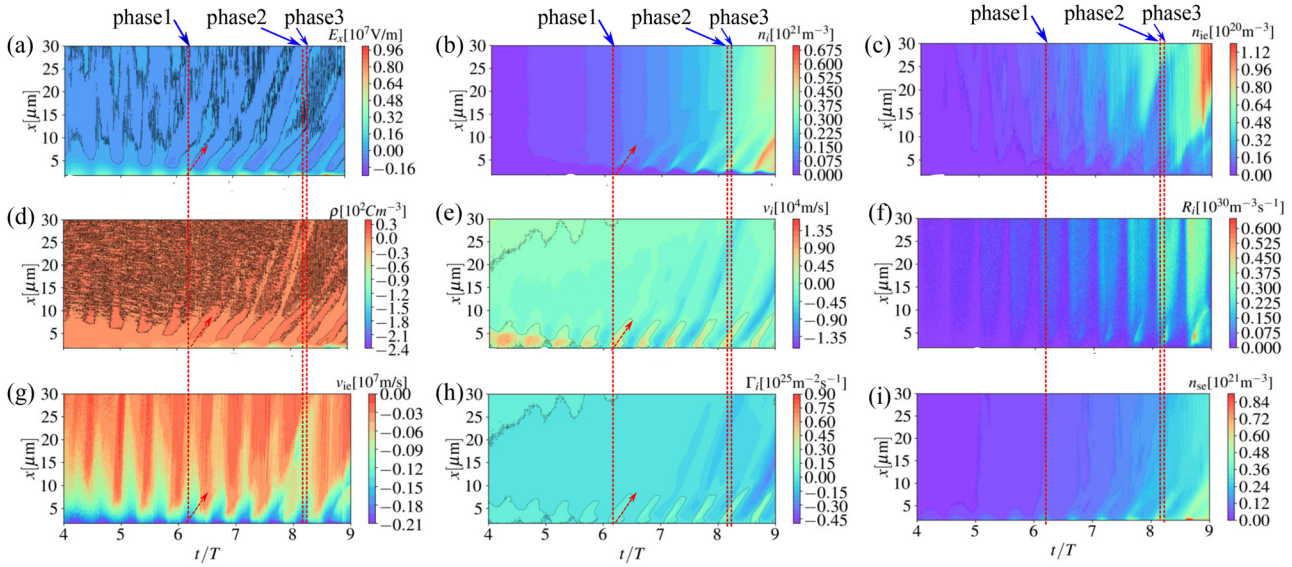

FIG. 3. Transient plasma physics for MSD based on proton mass and helium chemistry. Spatiotemporal plots of the (a) electric field, (b) ion density, (c) ionization electron density, (d) net charge density, (e) ion fluid velocity, (f) ionization rate, (g) ionization electron velocity, (h) ion flux, and (i) secondary electron density. Phases 1, 2, and 3 represent the moment $t/T \approx 6.15, 8.13$, and 8.16, separately. The black dashed line indicates the value of zero in (a), (d), (e), and (h).

$t/T \approx 6.5$ [see Figs. 3(c), 3(f), 3(g), and 3(i)], i.e., the formation of the ion pattern is prior to that of the electron pattern, suggesting that ion dynamic is responsible for triggering the MSD.

The detailed ion dynamics is revealed by the ion density, ion flux, net charge density, and normal electric field, whose normalized spatial distributions at the moment when MSD is triggered, phase 1, are shown in Fig. 4(a). As we mentioned above, the normal electric field, E_x, is positive near the surface (purple region) due to multipactor in region I, where the emitted secondary electrons make the net charge negative [also see Figs. 3(a) and 3(d)]. In region II adjacent to the bulk plasma, E_x is negative due to electron-ion ambipolar diffusion. Under the action of E_x in region II, the ion flux $\Gamma_i < 0$ [also see Fig. 3(h)] and decreases first and then increases with a transition at location $x = x_2$, where $E_x = 0$. Due to inertia, the ions still flow collectively toward the surface within the region of $x_1 < x < x_2$ with x_1, where $\Gamma_i = 0$. In the region $x < x_1$, the ions flow away from the surface. Therefore, the ion density is significantly enhanced at x_1, giving rise to a prominent ion peak as the red line shows in Fig. 4(a). Within $T/2$, the multipactor discharge near the surface is further enhanced after phase 1, since the transverse ac electric field increases, which causes a higher electron impact energy and higher SEY. The normal electric field in region I also increases and pushes the local ion density peak away from the surface.

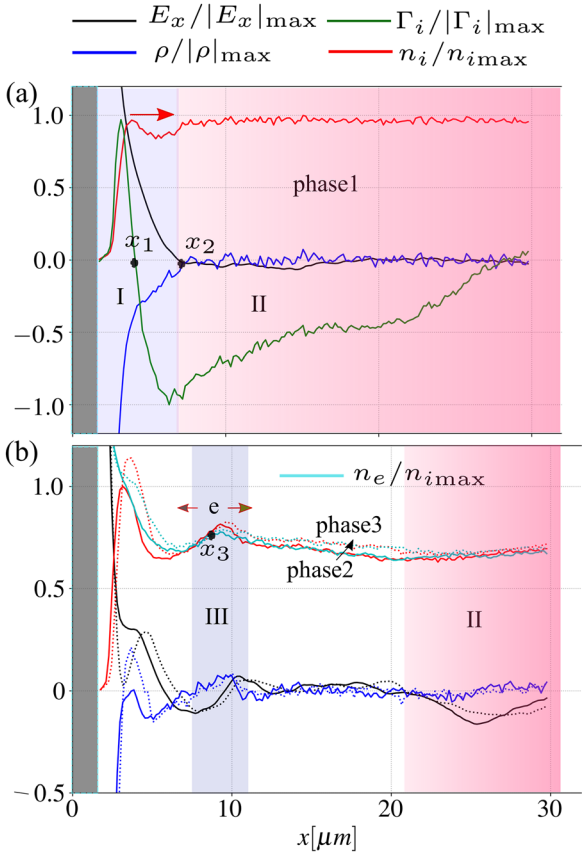

FIG. 4. The normalized spatial normal electric field (black line), ion flux (green line), net charge density (blue line), and ion density (red line), as well as the electron density (cyan line) as a function of distance, x, from the dielectric surface, for (a) phase 1 and (b) phase 2 (solid line) and phase 3 (dashed line). The normalized parameters are $|E|_{max} = 1.03 \times 10^6$ V/m, $\rho_{max} = 10.82\,\mathrm{Cm}^{-3}$, $|\Gamma_i|_{max} = 2.2 \times 10^{23}\,\mathrm{m}^{-2}\,\mathrm{s}^{-1}$, and $n_{imax} = 7.06 \times 10^{19}\,\mathrm{m}^{-3}$ for (a) and $|E|_{max} = 1.03 \times 10^6$ V/m, $\rho_{max} = 10.82\ \mathrm{Cm}^{-3}$, and $n_{imax} = 3.44 \times 10^{20}\ \mathrm{m}^{-3}$ for (b).

After the first locally high ion density wave is generated and gradually moves away from the surface, the electrons are attracted by the local ion potential well and follow the motion of ions. Therefore, the locally high electron density for both ionization and secondary electrons is also gradually formed as shown in Figs. 3(c) and 3(i). The locally peaked electron density induces a local peak for electron-neutral impact ionization rate [see Fig. 3(f)]. The locally high impact ionization frequency produces a locally high plasma density for both electrons and ions. Furthermore, the lighter electrons diffuse toward the bulk plasma (away from the surface). The diffusion of electrons toward the bulk plasma also drives the ion peak to propagate toward the bulk plasma region. The detailed dynamics of propagation is shown in Fig. 4(b) by tracing two adjacent instantaneous moments, $t/T = 8.13$ and 8.16, i.e., phase 2 and phase 3 as indicated by the red dashed line in Fig. 3. Phase 2 and phase 3 are two moments that can clearly show the multilayer structure. The total electron density n_e, the ion density n_i, the electric field E_x, and the total charge density ρ are plotted for phase 2 (solid line) and phase 3 (dashed line) vs x. Compared to Fig. 4(a), region II, within which an electric field is negative due to electron diffusion, is still present but closer to the bulk plasma. Region III with a local peak plasma density near $x = x_3$ appears closer to the surface. Comparing phases 2 to 3, although the peak electron density at x_3 contributes to the locally high ionization rate, the net gain of the electron density near x_3 is much smaller than that of both the left and right sides of region III. Hence the electrons are diffusing toward both sides of region III. When the electrons diffuse toward the left side, a net gain of the negative charge on the left side ($x < x_3$) will be obtained. Therefore, the electric field and net charge density are more negative on the left side of region III. On the other hand, when electrons diffuse toward the right side ($x > x_3$), the positive charge is left, and the electric field will become more positive.

The propagation of the positive electric field far away from the surface will promote the ion density peak to further propagate toward the bulk plasma in region III of Fig. 4(b). In addition to the ion density propagating in space, the distribution of the locally high ion density will be broader in time due to diffusion. As a result, only two remarkable ion density peaks are observed near phase 2 [also see Fig. 3(b)]. The other structures of the locally high ion density adjacent to the bulk plasma during phase 1 and phase 2 in Fig. 3(b) are nearly invisible due to their broader distribution [see the region between region III and region II in Fig. 4(b)]. It is worth noting that both the secondary electron emission from the surface and the electron impact ionization would not contribute to the net gain of charge, since ionization electrons and ions, surface-emitted electrons, and resident positive charge on the surface equally increase to keep overall charge neutrality in the system. The lighter electron diffusion induced ambipolar field toward the bulk plasma is mainly responsible for the propagation of the multilayer structure.

In summary, we studied the formation of a MSD for the normal electric field and plasma density in the early stage of multipactor-coexisting plasma breakdown in helium gas, reported near a high-power microwave window. The multipactor-ionization breakdown process near the microwave window has been a key limiting factor in rf and microwave devices, especially for the next generation of

communication satellite design, which requires higher microwave power. Therefore, understanding the transient breakdown process is of importance for further optimizing and controlling signal generation in the complicated helium/hydrogen-containing space environment. By further investigation into a proton mass system, where the multilayer structure is enhanced with electron-relevant processes for He kept unchanged, the mechanism of the multilayer generation is attributed to the local ion density enhancement under two neighboring electric fields acting in opposite directions. The electrons locally diffuse away from the surface, resulting in a local ambipolar field pointing toward the bulk plasma, which drives the ion density peak toward the bulk plasma. Such a process is periodically repeated, resulting in MSD formation. When a MSD is formed, the local density near the dielectric surface will be extremely high for a short period of time. As a result, the discharge is locally enhanced near the dielectric surface in this period and induces a faster ionization breakdown. The MSD reported in our work shows a fundamental mechanism that prompts ionization breakdown within a few layers near the rf window surface. The understanding of the breakdown mechanism enables researchers to optimize space-based high-power microwave systems. The MSD structures are expected to vary for different driving frequencies, dielectric surface materials, and ion masses in space-based microwave systems. Comparative studies under different conditions merit further investigation and will be presented in the future work. In addition, experimental evidence on the MSD is also expected in helium or hydrogen background gas, and the MSD may be observed via nanosecond response intensified charged-couple device cameras[15] with high spatial resolution, where a few discrete regions may show layered light intensity and the light intensity would be more significant near the dielectric surface than the plasma region away from the surface in the early stage of the plasma breakdown.

See the supplementary material for the evolution of the spatial electron and ion density profile in time and also for the propagating behavior of a multilayer-structured discharge.

The authors are grateful to Professor Hae June Lee of Pusan National University for a fruitful discussion and to Professor Michael A. Lieberman and Dr. Emi Kawamura of U.C. Berkeley and Professor Jon Gudmundsson of University of Iceland for discussions about benchmarking the PIC code. This work was supported by the Air Force Office of Scientific Research (AFOSR) MURI under Grant No. FA9550-18-1-0062 and AFOSR under Grant No. FA9550-21-1-0367. Y. F. acknowledges the support from the Tsinghua University Initiative Scientific Research Program and the State Key Laboratory of Power System and Generation Equipment (Project No. SKLD21M06).

AUTHOR DECLARATIONS

Conflict of Interest

The authors have no conflicts to disclose.

DATA AVAILABILITY

The data that support the findings of this study are available from the corresponding author upon reasonable request.

REFERENCES

[1]M. Lieberman and A. Lichtenberg, *Principles of Plasma Discharges and Materials Processing*, 2nd ed. (Wiley, New York, 2005).
[2]J. Power, W. Gai, S. Gold, A. Kinkead, R. Konecny, C. Jing, W. Liu, and Z. Yusof, Phys. Rev. Lett. **92**, 164801 (2004).
[3]Y. Hidaka, E. Choi, I. Mastovsky, M. Shapiro, J. Sirigiri, and R. Temkin, Phys. Rev. Lett. **100**, 035003 (2008).
[4]S. K. Nam and J. P. Verboncoeur, Phys. Rev. Lett. **103**, 055004 (2009).
[5]J.-P. Boeuf, B. Chaudhury, and G. Q. Zhu, Phys. Rev. Lett. **104**, 015002 (2010).
[6]R. A. Kishek and Y. Y. Lau, Phys. Rev. Lett. **75**, 1218 (1995).
[7]R. A. Kishek and Y. Y. Lau, Phys. Rev. Lett. **80**, 193 (1998).
[8]R. A. Kishek, Y. Y. Lau, L. K. Ang, A. Valfells, and R. M. Gilgenbach, Phys. Plasmas **5**, 2120 (1998).
[9]S. C. Schaub, M. A. Shapiro, and R. J. Temkin, Phys. Rev. Lett. **123**, 175001 (2019).
[10]H. Wang, D. Liu, L. Liu, M. Xie, and L. Meng, Plasma Sources Sci. Technol. **27**, 125006 (2018).
[11]H. Wang, D. Liu, L. Liu, and L. Meng, Plasma Sources Sci. Technol. **29**, 037001 (2020).
[12]A. Valfells, L. K. Ang, Y. Y. Lau, and R. M. Gilgenbach, Phys. Plasmas **7**, 750 (2000).
[13]A. Valfells, J. P. Verboncoeur, and Y. Y. Lau, IEEE Trans. Plasma Sci. **28**, 529 (2000).
[14]R. A. Kishek, Phys. Rev. Lett. **108**, 035003 (2012).
[15]C. Chang, M. Zhu, J. Verboncoeur, S. Li, J. Xie, K. Yan, T. Luo, and X. Zhu, Appl. Phys. Lett. **104**, 253504 (2014).
[16]P. Y. Wong, Y. Y. Lau, P. Zhang, N. Jordan, R. M. Gilgenbach, and J. Verboncoeur, Phys. Plasmas **26**, 112114 (2019).
[17]A. Iqbal, J. Verboncoeur, and P. Zhang, Phys. Plasmas **25**, 043501 (2018).
[18]H. C. Kim and J. P. Verboncoeur, Phys. Plasmas **12**, 123504 (2005).
[19]D.-Q. Wen, P. Zhang, Y. Fu, J. Krek, and J. P. Verboncoeur, Phys. Plasmas **26**, 123509 (2019).
[20]A. Iqbal, J. Verboncoeur, and P. Zhang, Phys. Plasmas **26**, 024503 (2019).
[21]S. Michizono, Y. Saito, S. Yamaguchi, and S. Anami, IEEE Trans. Electr. Insul. **28**, 692 (1993).
[22]A. Neuber, J. Krile, G. Edmiston, and H. Krompholz, Phys. Plasmas **14**, 057102 (2007).
[23]J. Foster, M. Thomas, and A. Neuber, J. Appl. Phys. **106**, 063310 (2009).
[24]C. Chang, G. Liu, C. Tang, C. Chen, H. Shao, and W. Huang, Appl. Phys. Lett. **96**, 111502 (2010).
[25]D.-Q. Wen, A. Iqbal, P. Zhang, and J. P. Verboncoeur, Phys. Plasmas **26**, 093503 (2019).
[26]P. Zhang, Y. Y. Lau, M. Franzi, and R. M. Gilgenbach, Phys. Plasmas **18**, 053508 (2011).
[27]H. C. Kim and J. P. Verboncoeur, Phys. Plasmas **13**, 123506 (2006).
[28]A. Neuber, G. Edmiston, J. Krile, H. Krompholz, J. Dickens, and M. Kristiansen, IEEE Trans. Magn. **43**, 496 (2007).
[29]Y. Y. Lau, J. P. Verboncoeur, and H. C. Kim, Appl. Phys. Lett. **89**, 261501 (2006).
[30]D. J. McComas, S. J. Bame, B. L. Barraclough, W. C. Feldman, H. O. Funsten, J. T. Gosling, P. Riley, R. Skoug, A. Balogh, R. Forsyth *et al.*, Geophys. Res. Lett. **25**(1), 1–4, https://doi.org/10.1029/97GL03444 (1998).
[31]S. Bourdarie and M. Xapsos, IEEE Trans. Nucl. Sci. **55**, 1810 (2008).
[32]D. Garoli, L. V. Rodriguez De Marcos, J. I. Larruquert, A. J. Corso, R. P. Zaccaria, and M. G. Pelizzo, Appl. Sci. **10**, 7538 (2020).
[33]M. T. P. Aldan, Ph.D. thesis, University of California at Berkeley, 2015.
[34]A. Neuber, D. Hemmert, H. Krompholz, L. Hatfield, and M. Kristiansen, J. Appl. Phys. **86**, 1724 (1999).
[35]J. T. Gudmundsson, E. Kawamura, and M. A. Lieberman, Plasma Sources Sci. Technol. **22**, 035011 (2013).
[36]D.-Q. Wen, J. Krek, J. T. Gudmundsson, E. Kawamura, M. A. Lieberman, and J. P. Verboncoeur, Plasma Sources Sci. Technol. **30**, 105009 (2021).
[37]M. M. Turner, A. Derzsi, Z. Donkó, D. Eremin, S. J. Kelly, T. Lafleur, and T. Mussenbrock, Phys. Plasmas **20**, 013507 (2013).
[38]V. Vahedi, C. K. Birdsall, M. A. Lieberman, G. DiPeso, and T. D. Rognlien, Plasma Sources Sci. Technol. **2**, 273 (1993).

[39]A. Iqbal, P. Y. Wong, D.-Q. Wen, S. Lin, J. Verboncoeur, and P. Zhang, Phys. Rev. E **102**, 043201 (2020).
[40]J. Zhang, W. Luo, M. Jiang, H. Wang, Y. Li, and C. Liu, Plasma Sources Sci. Technol. **29**, 025013 (2020).
[41]V. Vahedi and M. Surendra, Comput. Phys. Commun. **87**, 179 (1995).
[42]J. T. Gudmundsson and M. A. Lieberman, Phys. Rev. Lett. **107**, 045002 (2011).
[43]J. R. M. Vaughan, IEEE Trans. Electron Devices **40**, 830 (1993).